Materials and Design 47 (2013) 243–247

Contents lists available at SciVerse ScienceDirect

Materials and Design

journal homepage: www.elsevier.com/locate/matdes

Technical Report

Friction stir welding of SiCp/2009Al composite plate

D. Wang [a], B.L. Xiao [a,*], Q.Z. Wang [a], Z.Y. Ma [a,b]

[a] Shenyang National Laboratory for Materials Science, Institute of Metal Research, Chinese Academy of Sciences, 72 Wenhua Road, Shenyang 110016, China
[b] State Key Laboratory of Metal Matrix Composites, Shanghai Jiao Tong University, 800 Dongchuan Road, Shanghai 200240, China

ARTICLE INFO

Article history:
Received 3 August 2012
Accepted 28 November 2012
Available online 8 December 2012

ABSTRACT

Six milimeter thick hot-rolled SiCp/2009Al composite plates were successfully joined by friction stir welding (FSW) using an ultra-hard material tool. After FSW, the distribution of the SiC particles in the nugget zone (NZ) was more homogeneous than that in the base material (BM). Scanning electron microscopic examinations (SEM) and X-ray analysis (XRD) indicated that part of the Al_2Cu was dissolved into the aluminum matrix in the NZ due to intense plastic deformation and high temperature during FSW. The undissolved Al_2Cu particles remained in the NZ and coarsened during the cooling process after FSW. The ultimate tensile strength (UTS) of the as-welded joint is only 321 MPa and failed in the BM zone due to the low strength of the BM. After T4 heat treatment, the strength of the joint increased and became close to that of the BM with T4 temper, because most of the Al_2Cu particles were dissolved into the matrix and re-precipitated homogeneously as the GP zones, which are the major strengthening precipitates for T4-tempered 2009Al alloy.

1. Introduction

Discontinuously reinforced metal matrix composites (DRMMCs) are attractive materials in the aerospace, instruments and automotive industrial fields due to their improved specific stiffness, strength, and superior wear resistance [1]. However, the poor weldability of these composites by conventional fusion welding techniques limits their industrial applications. Drawbacks such as the incomplete mixing of the parent and filler materials, eutectic formation, and the presence of porosity often occur in the fusion zone [2–4].

Friction stir welding (FSW), a solid-state joining technique, is considered a promising welding method for joining the DRMMCs to avoid the drawbacks of fusion welding [3]. In the last few years, a number of investigations have been conducted to join the DRMMCs by FSW [5–9]. It was reported that FSW could effectively improve the microstructure of DRMMCs such as Al_2O_3p/6061Al, SiCp/2009Al, and SiCp/2124Al composites [10–12]. The particle clusters, which were often observed in the composites, were broken up and the particle distribution became more homogeneous in the nugget zone (NZ) due to the intense plastic deformation and material mixing [10,11]. Furthermore, the stirring and breaking effect of the tool during FSW resulted in the breakup of the reinforcing particles and knocking-off of sharp corners and edges of the large particles, thereby changing the size and shape of the particles in the NZ [12–14].

However, two important challenges must be faced when welding the DRMMCs. Firstly, the DRMMCs exhibit much lower ductility than monolithic alloys even at high temperatures. Thus, the welding parameters are generally limited to high heat-input conditions, and welding defects are easily formed at lower heat input. Ceschini et al. [15] reported the formation of welding defects in the NZ resulting from the high traverse speed of 300 mm/min in Al_2O_3p/7075Al. Secondly, severe wear of the steel tool occurred during FSW due to the presence of hard ceramic reinforcements [16,17]. This not only reduced the lifetime of the tool, but also affected the properties of the FSW joints adversely, due to the existence of the wear debris. Feng et al. [11] reported that the intermetallics generated due to the wearing of the steel tool decreased the ultimate tensile strength (UTS) of FSW SiCp/2009Al joints.

Recently, Marzoli et al. [10] reported that FSW Al_2O_3p/6061Al joints were obtained by using an ultra-hard material tool. The UTS of the joints was lower and was only 70% of that of the base material (BM), with failure occurring in the heat affected zone (HAZ), which was the lowest hardness zone. However, no detailed microstructure of the joints responsible for the mechanical properties and fracture behavior of the joints were reported.

In this study, an ultra-hard material tool was used to join hot-rolled SiCp/2009Al plate by FSW and subsequent heat treatment of the FSW joint was conducted. The aim was to understand the effect of the FSW condition and post-FSW heat treatment on the microstructure and mechanical properties of the joints without tool wear debris.

* Corresponding author. Tel./fax: +86 24 83978630.
E-mail address: blxiao@imr.ac.cn (B.L. Xiao).

0261-3069/$ - see front matter © 2012 Elsevier Ltd. All rights reserved.
http://dx.doi.org/10.1016/j.matdes.2012.11.052

2. Experimental details

Six milimeter thick plates of 15 vol.% SiCp/2009Al composite plates, produced by powder metallurgy and subsequent hot rolling, were cut into $6 \times 75 \times 300$ mm along the rolling direction. The plates were friction stir butt welded along the rolling direction at a welding speed of 100 mm/min and a tool rotation rate of 800 rpm. An ultra-hard material tool with a shoulder 20 mm in diameter and a cylindrical pin 8 mm in diameter and 5.8 mm in length was used. After welding, the joints were naturally aged for seven days. To study the effect of post-weld heat treatment, some of the FSW samples were T4-treated (solutionized at 516 °C for 1 h, water quenched, and aged at room temperature for seven days). The as-FSW joint and T4-treated joint were named as-FSW and FSW-T4, respectively.

The joints were cross-sectioned perpendicular to the welding direction for optical microscopic (OM) and scanning electron microscopic (SEM) examinations. X-ray analysis (XRD) was conducted on a D/max 2500PC diffractometer at 50 kV and 250 mA, using Cu Kα radiation. The Vickers hardness profiles of the welds were measured on the cross section along the mid-thickness of the welded plates. Dog-bone-shaped tensile specimens with a gauge length of 40 mm and a width of 10 mm were machined perpendicular to the welding direction with the NZ being in the center of the gauge. The tensile properties were tested at a strain rate of $1 \times 10^{-3}\ s^{-1}$ by using an SHIMADZU AG-100KNG testing machine. The fracture surfaces of the tensile specimens were observed under an SEM.

3. Results and discussion

Fig. 1 shows a macrograph of the FSW SiCp/2009Al composite plate. No defects were detected in the joint, indicating that sound joining was achieved using the hard tool. The surface of the joint was smooth and characterized by semicircular patterns, similar to those observed in FSW monolithic Al alloys [18].

Fig. 2a and b shows the OM microstructure of the SiCp/2009Al composite perpendicular to the rolling direction and along the rolling direction, respectively. The SiC particles were homogeneously distributed on the cross section perpendicular to the rolling direction (Fig. 2a). However, some large SiC particles tended to be distributed along the rolling direction (Fig. 2b). The long axis of the SiC particles was usually distributed along the rolling direction in the composite plates, which results in the size diversity of the SiC particles observed in different directions.

In the as-FSW sample (Fig. 2c), the SiC particles were homogeneously distributed in the NZ. However, some large SiC particles were present in the NZ which were not observed in the BM perpendicular to the rolling direction (Fig. 2a). In the FSW process, the SiC particles flowed and rotated with the matrix due to the stirring by the welding tool [11,12]. Therefore, the SiC particles would be distributed randomly rather than directionally along the rolling direction. Therefore, some large SiC particles could be observed on the cross section of the NZ. For the FSW-T4 sample (Fig. 2d), the distribution of SiC particles in the NZ is similar to that of the as-FSW sample. This indicates that the T4-heat treatment did not change the distribution of SiC particles.

Fig. 1. Macrograph of FSW SiCp/2009Al composite.

Fig. 3a shows the backscattered electron (BSE) image of the BM. Many fine white particles were homogeneously distributed in the matrix. These particles were too small to be analyzed by the EDS. There were also some large white particles in the matrix. EDS analyses indicated that the irregular particles (marked "A") contained 79.12 Al, 10.58 Cu, 7.7 Si, 1.89 Mg, and 0.71 Fe (at.%) and the circular particles (marked "B") contained 84.42 Al, 10.51 Cu, 2.91 Si, 2.17 Mg (at.%). The XRD results (Fig. 4) revealed the existence of many Al_2Cu phases in the BM. This indicates that both the fine and circular shape particles in the BM, observed by SEM, were Al_2Cu phase. The phases containing Fe element were not detected in the XRD pattern due to their limited quantity.

The Fe element would be introduced to the matrix during the fabrication process of the composite and form Al_7Cu_2Fe intermetallic compound. In the hot rolling and subsequent cooling process, the Al_2Cu phase nucleated and grew on the Al_7Cu_2Fe particles [19]. Finally, irregular particles formed in the matrix. Furthermore, some Al_2Cu also nucleated in the matrix in the rolling process and formed the coarse circular Al_2Cu particles.

Fig. 3b shows the BSE image of the NZ in the as-FSW sample. The number of both fine and coarse particles in the NZ decreased compared to that in the BM. Moreover, the XRD result indicated that the Al_2Cu phase was also present in the NZ (Fig. 4). This means that most of the white particles observed in the NZ of the as-FSW sample were Al_2Cu. However, the height of the Al_2Cu peaks in the NZ in the XRD profile is visibly lower than that in the BM, indicating that the amount of the Al_2Cu phases in the as-FSW sample was lower than that in the BM. This is consistent with the SEM observations.

Jariyaboon et al. [20] measured the peak temperature distribution during FSW of 2024Al-T351 alloy. They found that the temperatures adjacent to the NZ were 480 °C. Mahoney et al. [21] reported that the temperature adjacent to the NZ was 420–470 °C during FSW of 7075Al-T651 alloy. For the SiCp/2009Al composite, the peak temperature of the NZ during FSW was possibly similar to the above temperature. It is believed that the intense plastic deformation in the NZ during FSW would accelerate the dissolution of the Al_2Cu particles. In addition, some large Al_2Cu particles would be broken up. However, the time of welding was short and some Al_2Cu would remain in the matrix. After welding, part of the dissolved Al_2Cu would re-precipitate in the NZ during the cooling process. Thus, some Al_2Cu particles were observed in the NZ of the as-FSW sample, but they were reduced in number compared to those in the BM.

In the FSW-T4 sample, the fine particles which were observed in the as-FSW sample disappeared and the number of coarse particles clearly decreased (Fig. 3c). The shape of the remaining particles was basically circular and irregular particles were hardly found. The EDS results suggested that most of the coarse particles contained Fe element. The XRD result shows that few peaks of Al_2Cu were present in the FSW-T4 sample (Fig. 4), which means that there were few Al_2Cu particles in the matrix. After the solution treatment, most of the Al_2Cu phases were dissolved. Similar to the BM [19], the GP zones were precipitated in the matrix during the natural aging process. Therefore, it was not easy to detect the Al_2Cu phase by either SEM or XRD. The undissolved Al_2Cu around the Al_7Cu_2Fe formed the coarse circular particles in the matrix.

Fig. 5 shows the hardness profile of the as-FSW and FSW-T4 samples on the cross section along the mid-thickness of the joints. For the as-FSW sample, the NZ exhibited hardness values of $\sim$150 HV with a width of about 13 mm. Furthermore, the advancing side (AS) of the NZ had a higher hardness value than the retreating side (RS). Beyond the NZ, the hardness decreased

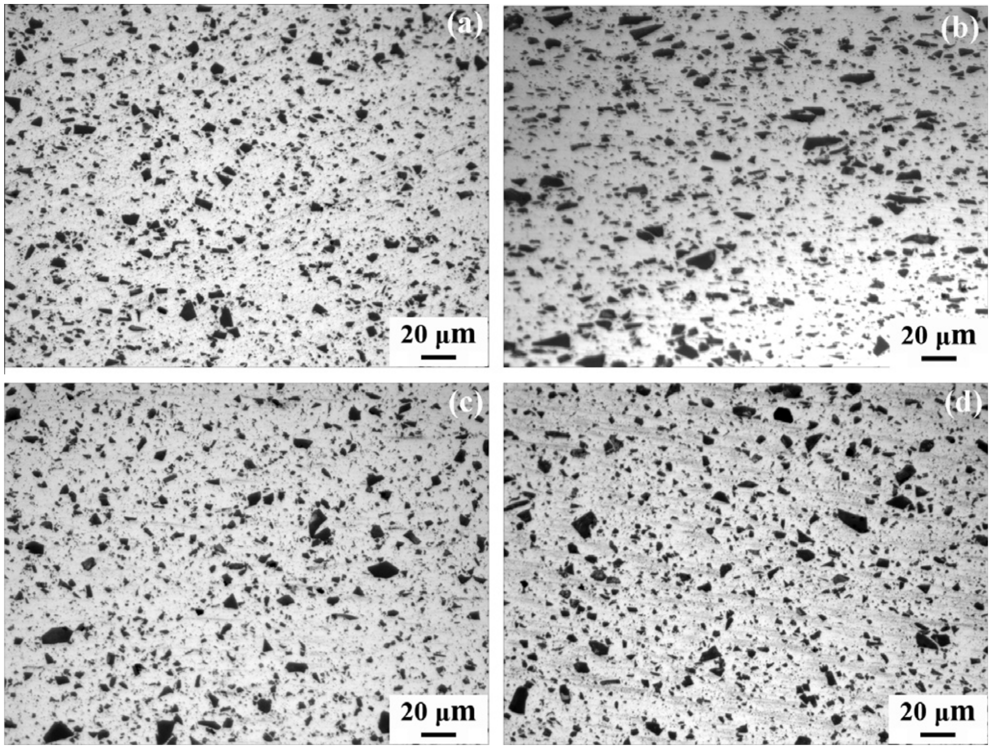

Fig. 2. Optical micrographs showing SiC particle distribution in (a) BM perpendicular to the rolling direction, (b) BM along the rolling direction, (c) as-FSW, and (d) FSW-T4.

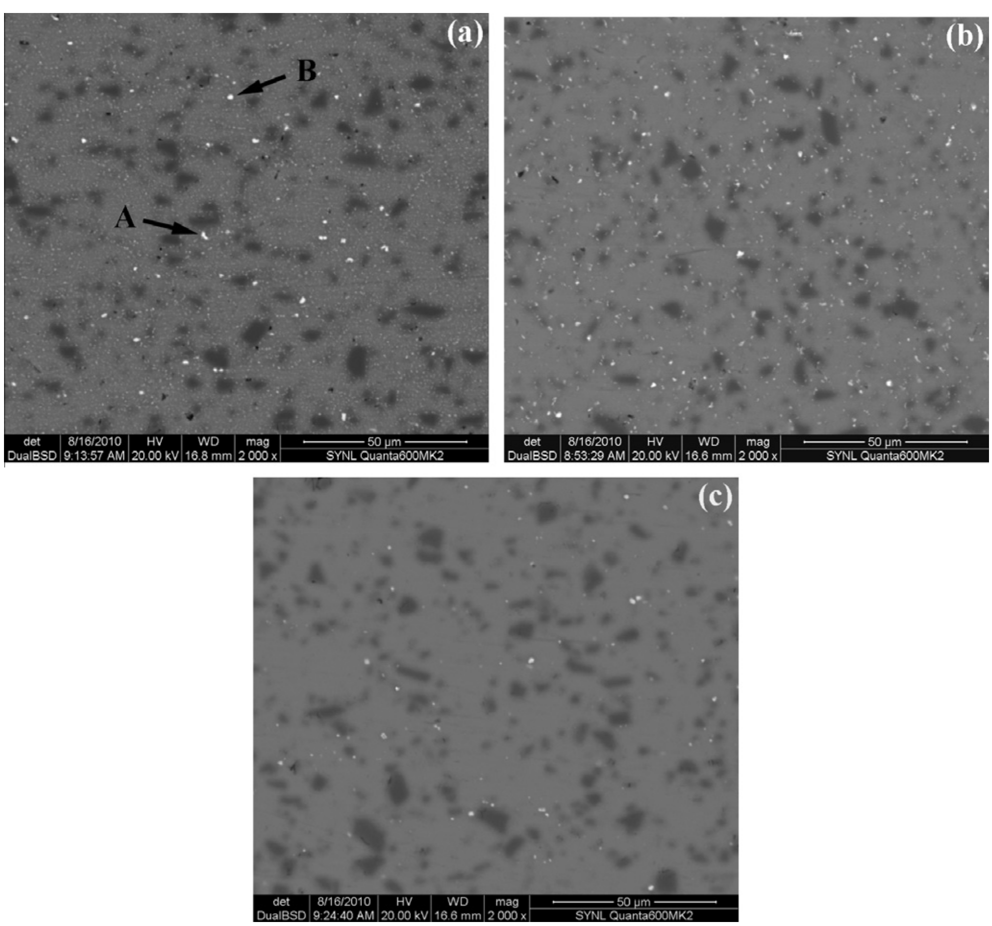

Fig. 3. Backscattered electron image of SiCp/2009Al composite: (a) BM, (b) as-FSW, and (c) FSW-T4.

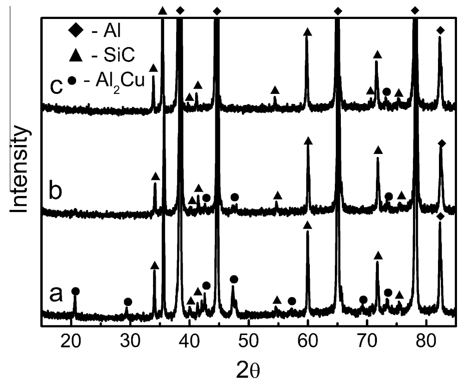

Fig. 4. XRD profiles of SiCp/2009Al composite: (a) BM, (b) as-FSW, and (c) FSW-T4.

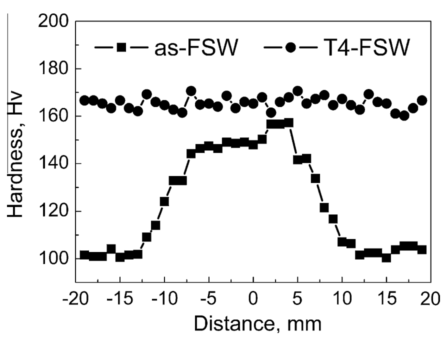

Fig. 5. Hardness profiles of FSW SiCp/2009Al composite.

Table 1
Tensile properties of SiCp/2009Al composite.

	YS (MPa)	UTS (MPa)	El. (%)
As-FSW	192	321	5.9
FSW-T4	344	521	7.1
BM-T4	357	543	13.1

gradually as the distance from the NZ increased. The hardness decreased to the level of the BM (∼100 HV) in the regions about 13 mm from the NZ center. For the FSW-T4 sample, both the BM and the various regions of the joint exhibited a similar hardness value of ∼170 HV.

In the FSW process, the NZ experienced intense plastic deformation and heating, resulting in the dissolution of most of the Al_2Cu. Fast cooling from the FSW temperature retained part of the solutes in solution, although some re-precipitation would occur during the cooling process of FSW. Then, the solutes precipitated as the GP zones during the natural aging process, increasing the hardness of the NZ significantly. In the HAZ, the dissolution of coarse Al_2Cu phases resulted in an increase in hardness compared to the BM. Therefore, the NZ had the maximum hardness. In addition, the AS of the NZ had a higher temperature than the RS due to severer deformation in this zone [1]. More Al_2Cu phases were dissolved in the matrix and more GP zones precipitated in this zone. Therefore, this zone had a higher hardness value compared to the other zones. For the FSW-T4 sample, the Al_2Cu phases were fundamentally dissolved during the solution treatment and then the GP zones precipitated during natural aging. This increased the hardness of the FSW joint significantly, so that it was close to that of the BM with T4 temper.

The ultimate tensile strength (UTS) of the as-FSW sample was 321 MPa (Table 1), with the joint failing in the BM zone far away from the NZ. The BM plate before welding was of hot rolled temper and had a low strength due to the coarse Al_2Cu phases as shown in Fig. 3a. Therefore, the FSW joint failed in the BM. Feng et al. [11] also reported that the FSW joint of as-extruded SiCp/2009Al composite welded by a steel tool failed in the BM zone.

The strength of the FSW-T4 sample was 521 MPa, and was enhanced significantly compared to that of the as-FSW sample. The sample failed in the NZ. Feng and Ma [7] reported that the Al_7Cu_2Fe formed in the NZ would decrease the strength of the T4-treated FSW SiCp/2009Al composite joints when steel tools were used. However, in this study, the welding tool was hard enough and almost no wearing occurred during FSW. Therefore, the FSW-T4 sample exhibited strength close to that of the T4-treated BM.

Fig. 6a shows an SEM micrograph of the tensile fracture surface of the as-FSW sample which failed in the BM zone with a 45 °C inclination to the tensile direction. The fracture surface was characterized by large dimples. Few SiC particles were observed on the fracture surface. The low strength of the matrix resulted in cracking of the matrix and the formation of many dimples on the fracture surface. With regard to the FSW-T4 sample (Fig. 6b), some fractured SiC particles were present on the fracture surface. The high strength of the matrix increased the possibility of SiC particle fracturing.

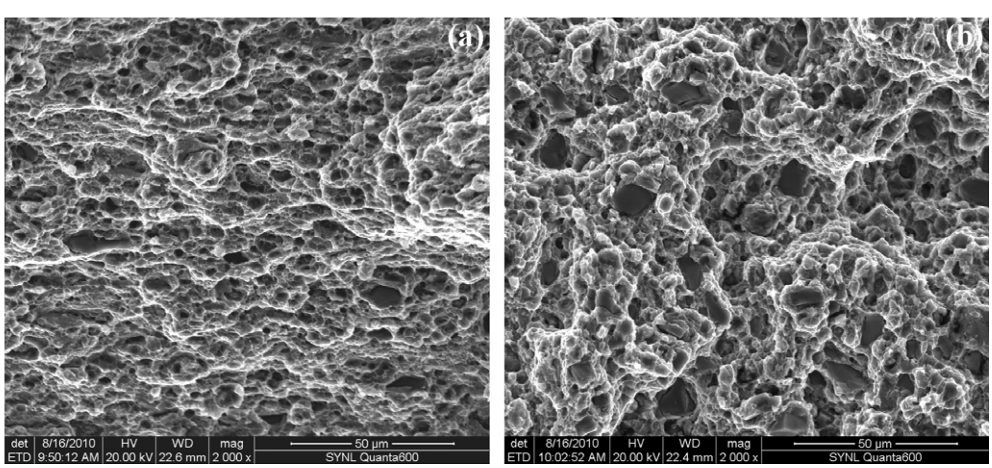

Fig. 6. SEM fractographs of FSW joints: (a) as-FSW and (b) FSW-T4.

4. Conclusions

In this study, the friction stir welding of 6 mm hot rolled 15 vol.% SiCp/2009Al composite was carried out using an ultra-hard material tool. The microstructure and mechanical properties of the joints were investigated. Some conclusions were achieved as follows.

(1) A defect-free FSW joint of 6 mm hot rolled 15 vol.% SiCp/2009Al composite was successfully obtained using an ultra-hard material tool.
(2) SiC particles were distributed more homogeneously in the NZ compared to those in the BM. Most Al_2Cu particles were dissolved and the remaining Al_2Cu particles became coarse in the NZ.
(3) The strength of the as-FSW joint was only 321 MPa and the joint failed in the BM zone due to the low strength of hot rolled temper. After T4-treatment, the strength of the joint increased up to 521 MPa, close to that of the BM with T4 temper.

Acknowledgments

The authors gratefully acknowledge the support of (a) the National Basic Research Program of China under Grant No. 2012CB619600 and (b) the State Key Laboratory of Metal Matrix Composites, Shanghai Jiao Tong University.

References

[1] Tjong SC, Ma ZY. Microstructural and mechanical characteristics of in situ metal matrix composites. Mater Sci Eng R 2000;29:49–113.
[2] Storjohann D, Barabash OM, Babu SS, David SA, Sklad PS, Bloom EE. Fusion and friction stir welding of aluminum-metal–matrix composites. Metall Mater Trans 2005;36:3237–47.
[3] Mishra RS, Ma ZY. Friction stir welding and processing. Mater Sci Eng R 2005;50:1–78.
[4] Wang XH, Niu JT, Guan SK, Wang LJ, Cheng DF. Investigation on TIG welding of SiCp-reinforced aluminum–matrix composite using mixed shielding gas and Al–Si filler. Mater Sci Eng A 2009;499:106–10.
[5] Nelson TW, Zhang H, Haynes T. Friction stir welding of aluminum MMC 6061-boron carbide. In: Proceedings of the second symposium on friction stir welding, Gothenburg, Sweden, June 2000.
[6] Prado RA, Murr LE, Shindo DJ, Sota KF. Tool wear in the friction-stir welding of aluminum alloy 6061 + 20% Al_2O_3: a preliminary study. Scr Mater 2001;45:75–80.
[7] Feng AH, Ma ZY. Formation of Cu_2FeAl_7 phase in friction-stir-welded SiCp/Al–Cu–Mg composite. Scr Mater 2007;57:1113–6.
[8] Gopalakrishnan S, Murugan N. Prediction of tensile strength of friction stir welded aluminium matrix TiCp particulate reinforced composite. Mater Des 2011;32:462–7.
[9] Nami H, Adgi H, Sharifitabar M, Shamabadi H. Microstructure and mechanical properties of friction stir welded Al/Mg_2Si metal matrix cast composite. Mater Des 2011;32:976–83.
[10] Marzoli LM, Strombeck AV, Dos Santos JF, Gambaro C, Volpone LM. Friction stir welding of an AA6061/Al_2O_3/20p reinforced alloy. Compos Sci Technol 2006;66:363–71.
[11] Feng AH, Xiao BL, Ma ZY. Effect of microstructural evolution on mechanical properties of friction stir welded AA2009/SiCp composite. Compos Sci Technol 2008;68:2141–8.
[12] Uzun H. Friction stir welding of SiC particulate reinforced AA2124 aluminium alloy matrix composite. Mater Des 2007;28:1440–6.
[13] Cavaliere P, Cerri E, Marzoli L, Santos JD. Friction stir welding of ceramic particle reinforced aluminium based metal matrix composites. Appl Compos Mater 2004;2:247–58.
[14] Srivatsan TS, Meslet AH, Petraroli M, Hotton B, Lam PC. Influence of silicon carbide particulate reinforcement on quasi static and cyclic fatigue fracture behavior of 6061 aluminum alloy composites. Mater Sci Eng A 2002;325:202–14.
[15] Ceschini L, Boromei I, Minak G, Morri A, Tarterini F. Effect of friction stir welding on microstructure, tensile and fatigue properties of the AA7005/10 vol.%Al_2O_3p composite. Compos Sci Technol 2007;67:605–15.
[16] Liu HJ, Fenga JC, Fujiib H, Nogi K. Wear characteristics of a WC-Co tool in friction stir welding of AC4A + 30 vol.%SiCp composite. Int J Mach Tool Manu 2005;45:1635–9.
[17] Shindo DJ, Rivera AR, Murr LE. Shape optimization for tool wear in the friction-stir welding of cast Al359-20% SiC MMC. J Mater Sci 2002;37:4999–5005.
[18] Cui GR, Ma ZY, Li SX. The origin of non-uniform microstructure and its effects on the mechanical properties of a friction stir processed Al–Mg alloy. Acta Mater 2009;57:5718–29.
[19] Rodrigo P, Poza P, Utrilla V, Urena A. Effect of reinforcement geometry on precipitation kinetics of powder metallurgy AA2009/SiC composites. J Alloy Compd 2009;479:451–6.
[20] Jariyaboon M, Davenport AJ, Ambat R, Connolly BJ, Williams SW, Price DA. The effect of welding parameters on the corrosion behaviour of friction stir welded AA2024-T351. Corros Sci 2007;49:877–909.
[21] Mahoney MW, Rhodes CG, Flintoff JG, Spurling RA, Bingel WH. Properties of friction-stir-welded 7075 T651 aluminum. Metall Mater Trans A 1998;29:1955–64.